ACSNANO
www.acsnano.org
ARTICLE

Multifunctional Dendrimer Ligands for High-Efficiency, Solution-Processed Quantum Dot Light-Emitting Diodes

Ikjun Cho,[†,∥] Heeyoung Jung,[‡,∥] Byeong Guk Jeong,[⊥] Jun Hyuk Chang,[#] Younghoon Kim,[†] Kookheon Char,[#] Doh C. Lee,[⊥] Changhee Lee,[‡] Jinhan Cho,[*,†] and Wan Ki Bae[*,¶]

[†]Department of Chemical and Biological Engineering, Korea University, Seoul 02841, Republic of Korea

[‡]School of Electrical and Computer Engineering, Inter-University Semiconductor Research Center and [#]School of Chemical and Biological Engineering, The National Creative Research Initiative Center for Intelligent Hybrids, Seoul National University, Seoul 08826, Republic of Korea

[⊥]Department of Chemical and Biomolecular Engineering, Korea Advanced Institute of Science and Technology (KAIST), Daejeon 34141, Republic of Korea

[¶]Photoelectronic Hybrids Research Center, Korea Institute of Science and Technology (KIST), Seoul 02792, Republic of Korea

Supporting Information

ABSTRACT: We present multifunctional dendrimer ligands that serve as the charge injection controlling layer as well as the adhesive layer at the interfaces between quantum dots (QDs) and the electron transport layer (ETL) in quantum dot light-emitting diodes (QLEDs). Specifically, we use primary amine-functionalized dendrimer ligands (*e.g.*, a series of poly(amidoamine) dendrimers (PADs, also referred to PAMAM)) that bind to the surface of QDs by replacing the native ligands (oleic acids) and also to the surface of ZnO ETL. PAD ligands control the electron injection rate from ZnO ETL into QDs by altering the electronic energy levels of the surface of ZnO ETL and thereby improve the charge balance within QDs in devices, leading to the enhancement of the device efficiency. As an ultimate achievement, the device efficiency (peak external quantum efficiency) improves by a factor of 3 by replacing the native ligands (3.86%) with PAD ligands (11.36%). In addition, multibranched dendrimer ligands keep the QD emissive layer intact during subsequent solution processing, enabling us to accomplish solution-processed QLEDs. The approach and results in the present study emphasize the importance of controlling the ligands of QDs to enhance QLED performance and also offer simple yet effective chemical mean toward all-solution-processed QLEDs.

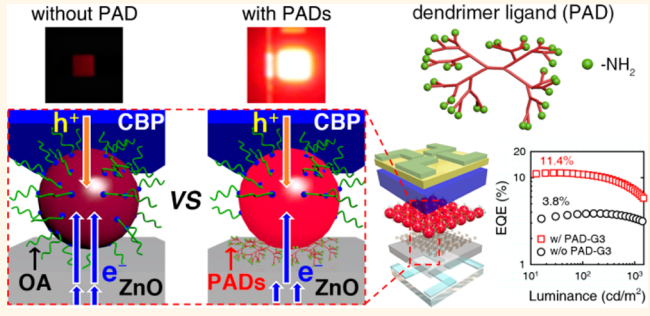

KEYWORDS: *dendrimer ligands, quantum dot-based light-emitting diode, charge injection, adhesive layer, interface engineering*

Nanocrystal quantum dots (QDs) exhibit narrow spectral emission bandwidth, emission wavelength tunability over the entire visible region, and near-unity photoluminescence quantum yield (PL QY),[1−4] calling attention to their utilization in a variety of light-emitting applications.[5−8] In addition, QDs are amenable to cost-efficient solution processing methods, suitable for optoelectronic applications. These advantages make QD-based light-emitting diodes (QLEDs),[5,9−14] in which QDs convert electrically injected charge carriers into photons, the most promising next-generation display technology following contemporary organic or inorganic light-emitting diodes.

In typical QLEDs, QD emissive layers are sandwiched between charge transport layers (CTLs) and electrodes.[9−12] QDs are typically formulated in a core/shell heterostructure and stabilized by long amphiphilic ligands (*e.g.*, oleic acid (OA)) during the synthesis. The presence of ligands is a double-edged sword for use of QDs in QLEDs. The ligands help disperse QDs in solvents and permit QD deposition on substrates *via* solution processing methods. In addition, the ligands can contribute to suppression of energy transfer among QDs by isolating QDs from neighboring ones, leading to an increase in the luminance efficiency of QD emissive layers. However, the long aliphatic ligands often hinder charge injection from CTLs into QDs, lowering the device perform-

Received: October 18, 2016
Accepted: December 14, 2016
Published: December 14, 2016

DOI: 10.1021/acsnano.6b07028
ACS Nano 2017, 11, 684−692

Scheme 1. (a) Schematic Illustration of the *in Situ* Ligand Exchange Process, (b) Chemical Structure (left) and Graphical Sketch (right) of PAD Ligands, and (c) Expanded Schematic of the Interface Between QDs and ZnO[a]

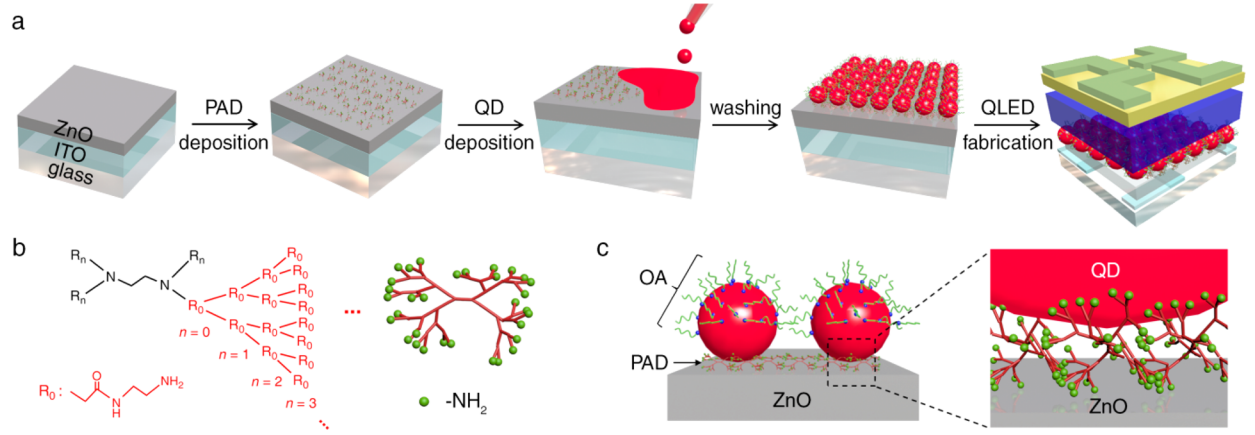

[a]Part of primary amine functional groups of PADs covalently coordinate to the surface of ZnO substrate and others anchor to the surface of QDs by removing weakly bound native ligands (*i.e.*, OAs) during the QD deposition.

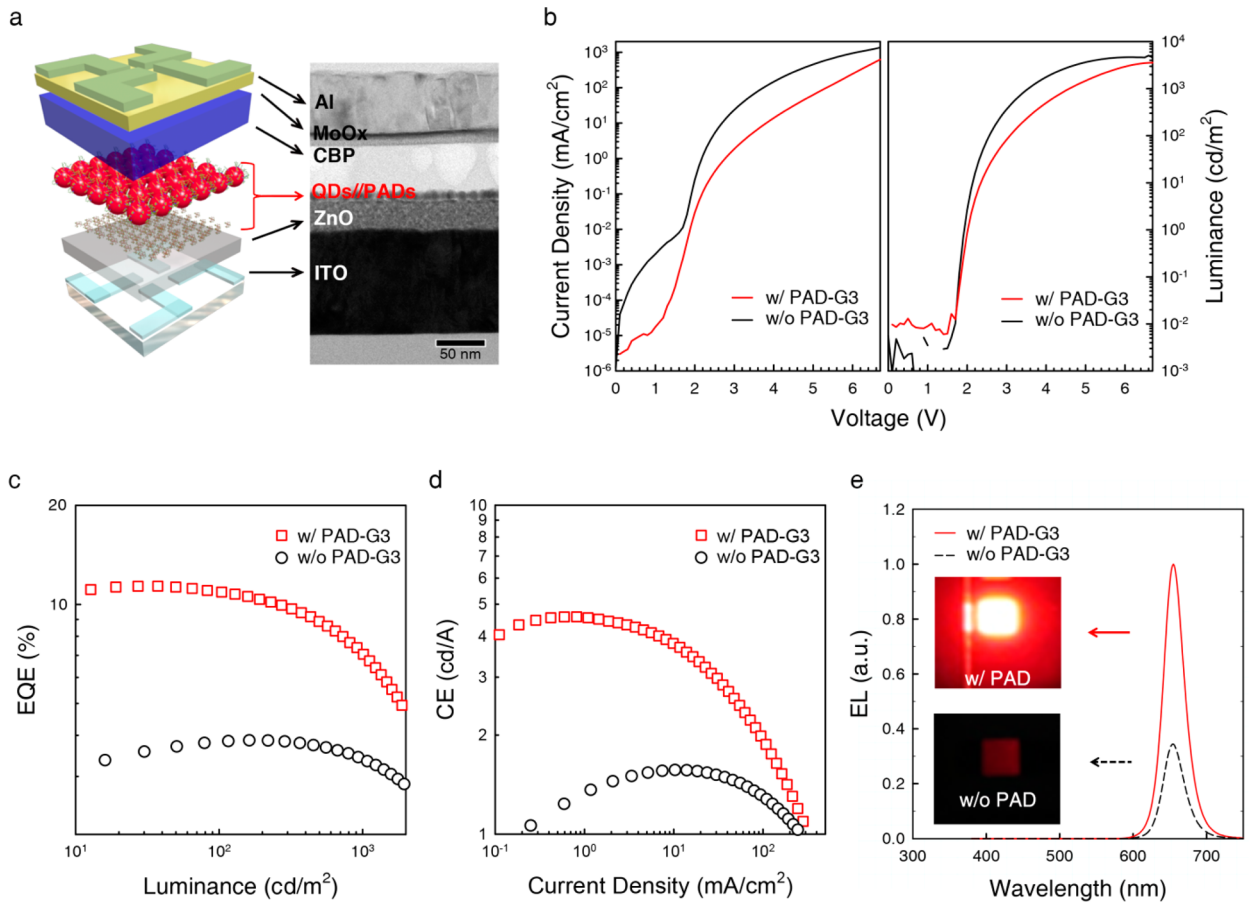

Figure 1. Device characteristics of QLEDs employing CdSe(r = 2 nm)/CdS(h = 6 nm) quasi-type II QDs with native ligands *versus* with multibranched dendrimer ligands. (a) Schematic illustration of inverted QLED (left) and the cross-sectional TEM image (right). (b) Current density−voltage−luminance characteristics, (c) EQE *versus* luminance, (d) CE *versus* luminance, and (e) EL spectra (at a current density of 10 mA/cm^2) and photographs (insets) of QLEDs with native ligands (w/o PAD-G3, black) and multibranched dendrimer ligands (w/PAD-G3, red).

ance.[15,16] In addition, the solubility of QDs conferred by ligand passivation makes the QD emissive layer vulnerable to uncontrollable dissolution during subsequent fabrication processes, ultimately narrowing the breadth of materials available for use as CTLs and electrodes.

Controlling the functions of ligands is expected to address these critical issues originating from the use of native aliphatic ligands (*e.g.*, OA).[17,18] Despite its importance and potential benefits, a systematic study on tailoring the ligands of QDs in relationship with the QLED performance has been lacking,

DOI: 10.1021/acsnano.6b07028
ACS Nano 2017, 11, 684−692

mostly deterred by the loss of luminance efficiency of the QD emissive layers, which frequently occurs during the ligand exchange processes and in turn harms the device efficiency.

In the present study, we demonstrate multifunctional dendrimer ligands for high-efficiency, solution-processed QLEDs. Specifically, we introduce primary amine-functionalized multibranched dendrimer ligands (*i.e.*, a series of poly(amidoamine) dendrimers (PADs or PAD-Gn (n = 0, 1, 3, 5), also referred to PAMAM)) that function as the charge injection controlling layer as well as the adhesive layer. The PAD ligands can effectively control the electron injection rate from ZnO ETL into QDs by shifting the energy level of ZnO ETL and thereby improve the charge balance within QDs in devices, leading to enhancement of the device efficiency. By replacing the native ligands with PAD ligands, the device efficiency (external quantum efficiency, EQE) is enhanced by a factor of 3 (from 3.86% to 11.36%). In addition, the modified dendrimer ligands keep the QD emissive layer intact during subsequent solution processing, enabling us to accomplish solution-processed QLEDs. The approach and results highlight the importance of interface engineering to enhance the QLED performance and also suggest the effective chemical tools for all-solution-processed QLEDs.

RESULTS AND DISCUSSION

Ligand modification often generates surface defects, which are effective nonradiative recombination centers particularly for core-only or thin-shell QDs.[18−21] Additionally, complete ligand exchange can shrink the mean QD-to-QD distance in films and result in increased energy transfer (ET) within QD films.[22] These changes can lower the film PL QY of QD emissive layers and the QLED device efficiency to a rather uncontrollable extent, complicating the interpretation of the influence of the ligands on the charge injection rate in relationship with the device performance. To avoid the difficulties, we used thick-shell QDs (*ca.* shell thickness ≥4 nm) (Figure S1−2),[19,23−26] in which the effect of surface defects on the exciton dynamics of the core is insignificant. In addition, we selectively replaced the native ligands (OA) of QDs on the side of the underlying CTL *via* the *in situ* ligand exchange reaction occurring during QD deposition (Scheme 1),[27,28] so that we could isolate the influence of ligand modification at the interface between QDs and CTL from variables originating from the morphological changes in QD emissive layers.

We chose inverted QLEDs with hybrid CTLs in a configuration of ITO//ZnO//QD emissive layer//4,4′-bis(*N*-carbazolyl)-1,1′-biphenyl (CBP)//MoO_x//Al as the testbed (Figure 1).[25,26] For these device structures, a 32 nm-thick ZnO ETL layer was first deposited onto patterned ITO//glass substrate by spin-casting a ZnO precursor and then annealing the film at 300 °C for 2 h (Experimental Methods section).[29] We employed 1-to-2-monolayer-thick QD emissive layers by spin-casting a QD dispersion on ZnO//ITO substrates. QLED fabrication was finalized by thermally evaporating a hole transport layer (HTL, CBP), hole injection layer (MoO_x), and Al on top of the QD emissive layer.

We introduced primary amine-functionalized multibranched dendrimer ligand layers (PADs, approximately 1 nm thick, Figure S3) at the interface between the ZnO ETL and QD emissive layers by spin-casting the PAD solutions on the top surface of the ZnO ETL prior to the QD deposition. Part of the primary amine functional groups covalently coordinates to the surface of ZnO ETL and others anchor to the surface of QDs on the other side by replacing the loosely bound native ligands (OA) during the spin-casting of QD emissive layers (Scheme 1, Figure S4). The outermost QD surface unbound to PAD ligands is still stabilized with OAs. Both the ligand modification layer and the QD emissive layer were washed with organic solvent after each deposition step to remove weakly bound ligands and QDs from the devices.

For ease of monitoring the changes in the electron injection rate, we first tested QLEDs with CdSe(radius (r) = 2.0 nm)/CdS(shell thickness (h) = 6 nm) core/shell heterostructured QDs, in which electrons can easily migrate between the CdSe core and ZnO ETL because the energetic barrier of the CdS shell is only 10−20 meV (Figure S1, Table 1).[24,25] Ligand

Table 1. Device Characteristics of QLEDs Employing CdSe(r = 2 nm)/CdS(h = 6 nm) Quasi-Type II QDs with Native Ligands (OA) and PAD-Gn (n = 0, 1, 3, and 5)[a]

QD	ligands	λ_{max}	V_{ON}	max EQE (%)	max CE (cd/A)	max PE (lm/W)	L (cd/m^2) @ 10 mA/cm^2
CdSe/CdS	OA	656	1.8	3.86	1.57	1.98	162.24
	PAD-G0	658	1.8	5.68	2.26	3.08	180.38
	PAD-G1	658	1.9	7.96	3.17	3.62	264.47
	PAD-G3	658	1.9	11.36	4.58	5.91	373.85
	PAD-G5	658	1.9	8.03	3.18	3.69	283.83

[a]Abbreviations: wavelength at the peak EL intensities (λ_{max}), turn-on voltage (V_{ON}), external quantum efficiency (EQE), current efficiency (CE), power efficiency (PE), and luminance (L).

modification from OA to PAD-Gn (n = 0, 1, 3, and 5) alters neither the morphology of QD emissive layers nor the structure of ZnO (Figure S4−S5). On the contrary, this exchange process has rather substantial impacts on the device performance. Specifically, the insertion of PAD ligands leads to suppression of the leakage current below the turn-on voltage (Figure 1b) and dramatic enhancement of the device efficiency (Figure 1c, Table 1, Figure S6). As an ultimate achievement, the EQE is enhanced by a factor of 3 after exchanging the native ligands (peak EQE = 3.86%) with PAD-G3 (peak EQE = 11.36%) and current efficiency (CE) is also increased from 1.57 cd/A to 4.58 cd/A (Figure 1c−e, Table 1). Given that the out-coupling efficiency of the QLED (η_{ext}) is 0.2, the ligand modification enhances the internal quantum efficiency (IQE, *ca.* 57%) of the device approximately up to the PL QY of the QD emissive film (61%), which is considered to be the limit of device efficiency.[30] The close connection between the device efficiency and the PL QY of the QD emissive layer signifies that the electron injection rate from ZnO into QDs harmonizes with the hole injection rate from CBP into QDs, so that the pairs of electrons and holes recombine in QD emissive layers as a case of photoexcitation. We note that, unlike the previous prediction,[31] the exciton dissociation by the external electric field in CdSe/CdS quasi-type II heterostructured QDs is not significant at the peak EQE condition.

To more concretely explore the role of the ligands, we characterized the optical properties of QD emissive layers and the device performance in relationship with the structure of multibranched dendrimer ligands (*e.g.*, the generation of dendrimers (G0-G5)) (Figure 2, Table 2) or the type of

DOI: 10.1021/acsnano.6b07028
ACS Nano 2017, 11, 684−692

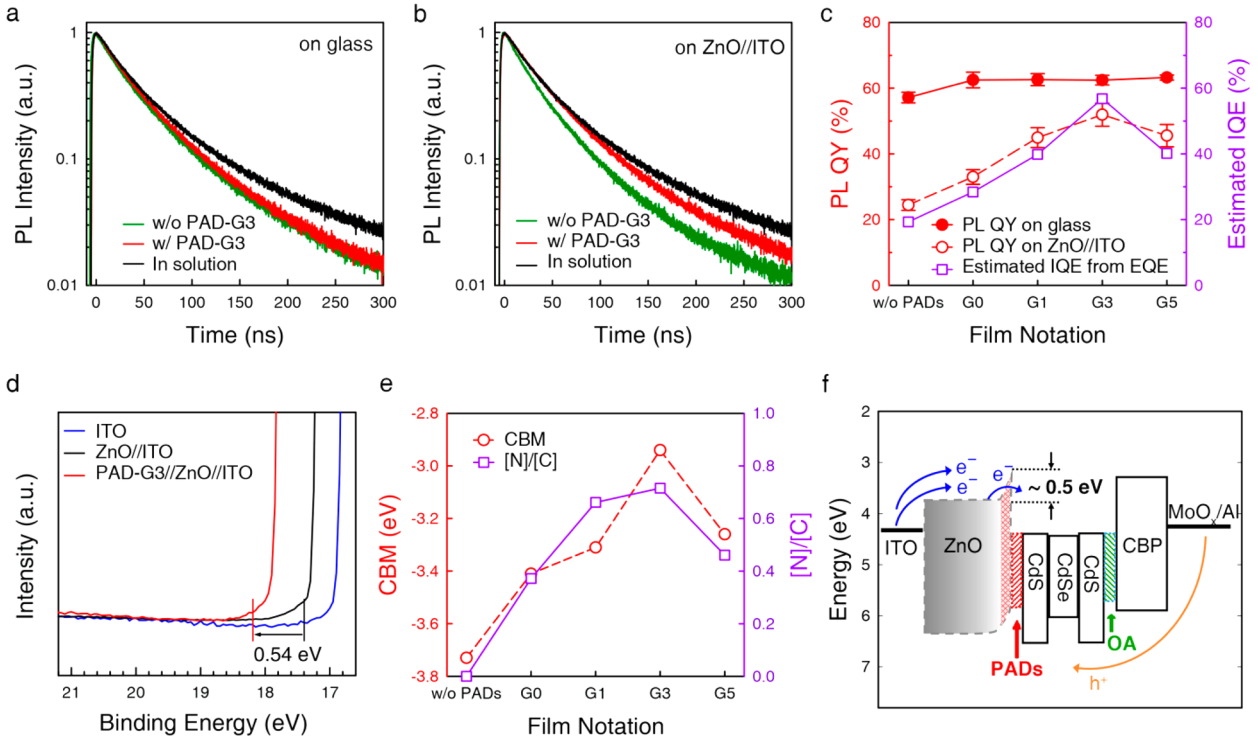

Figure 2. PL decay dynamics of QD films with native ligands (w/o PAD-G3, green) *versus* PAD-G3 (red) on (a) glass substrates and (b) ZnO//ITO//glass substrates. PL decay dynamics of QD solution (black) is overlaid for comparison. (c) Film PL QYs of QD emissive layers on glasses (red, filled circle), on ZnO//ITO//glass (red, empty circle) and the estimated IQE (purple, empty square) depending on the structure of the ligand modification layer. (d) Enlarged ultraviolet photoelectron spectra at the high binding energy regime of ITO (blue), ZnO//ITO film (black), and PAD-G3//ZnO//ITO film (red). (e) Conduction band minimum energy levels (CBM, red circle) and nitrogen/carbon ratios ([N]/[C] ratio, purple square) of ZnO depending on the structure of the ligand modification layer. The [N]/[C] ratio was measured using XPS analysis (see Figure S10). (f) Energy band diagram of QLEDs with PAD ligands.

Table 2. Electronic Energy Levels of the Surface of ZnO Films Depending on the Structure of PAD Ligands[a]

ligands	[N]/[C] ratio	VBM (eV)	E_F (eV)	CBM (eV)
none	0.00	6.95	3.83	3.71
PAD-G0	0.37	6.59	3.43	3.38
PAD-G1	0.66	6.53	3.41	3.30
PAD-G3	0.72	6.30	3.29	3.06
PAD-G5	0.46	6.50	3.37	3.24

[a]Abbreviations: valence band maximum (VBM), Fermi energy level of ZnO surfaces (EF), conduction band minimum (CBM), and [nitrogen]/[carbon] ratio ([N]/[C] ratio).

functional groups (*e.g.*, primary amine ($-NH_2$) *versus* carboxylic acid ($-COOH$) *versus* thiol ($-SH$)) (Figures S7–8). Because the mean QD-to-QD distance in QD emissive layers that determines the energy transfer (ET) rate remains unchanged through the ligand modification, the difference in the decay dynamics of QD emissive layers indeed reflects the changes in nonradiative recombination rates of QDs *via* surface trapping or Auger recombination (AR) processes.[32−35] The PL decay dynamics of QD emissive layers on glass substrates remain unchanged throughout the ligand modification process ($\tau_{1/e}$ = 42 ns, Figure 2a), indicating that surface defects, which affect the exciton dynamics, do not emerge during ligand modification. The PL decay dynamics become faster in contact with ZnO//ITO for pristine QDs ($\tau_{1/e}$ = 33 ns) as a result of negative charging of QDs with electrons that spontaneously migrate from the ZnO ETL. In contrast, the PL decay dynamics of QDs with amine-functionalized multibranched dendrimer ligands ($\tau_{1/e}$ = 42 ns) are less sensitive to contact with ZnO//ITO (Figure 2b), suggesting that spontaneous charging is suppressed as a consequence of the ligand modification. The tendencies observed in the device performance are in line with that from the optical properties of QD emissive layers (Figure 2c). The device efficiency is enhanced at most by a factor of 3 after modifying the native ligands with amine-functionalized dendrimer ones, implying that the charge balance within QDs in the actual working devices improves substantially.

Contrary to the case of primary amine-functionalized multibranched PAD ligands, the introduction of carboxylic acid- or thiol-functionalized multibranched ligands leads to a decrease in the device efficiency (Figure S8). The comparative experiments suggest that the type of functional groups, rather than the structure of ligands, is primarily associated with the enhanced charge balance within QDs at stationary or under operational conditions. For better understanding, we characterized the electronic energy levels of the surface of the ZnO ETL and QDs upon the ligand modification layers (Figure 2d). Ultraviolet photoelectron spectroscopy unveils that the conduction band edge energy level and the Fermi level of the surface of the ZnO ETL shift up by at most 0.5 eV as a consequence of the coordination of primary amine groups onto the surface of Zn atoms (Figure 2d, Table 2).[36,37] The coordination of primary amines creates an energetic barrier as high as 0.5 eV, which impedes electron injection from the side of ZnO//ITO to the QD emissive layers (Figure 2e, Figure S9). The alteration in the structure of PAD ligands varies the density of primary amine functional groups coordinating to the surface of ZnO and thereby the barrier height. It should be

DOI: 10.1021/acsnano.6b07028
ACS Nano 2017, 11, 684–692

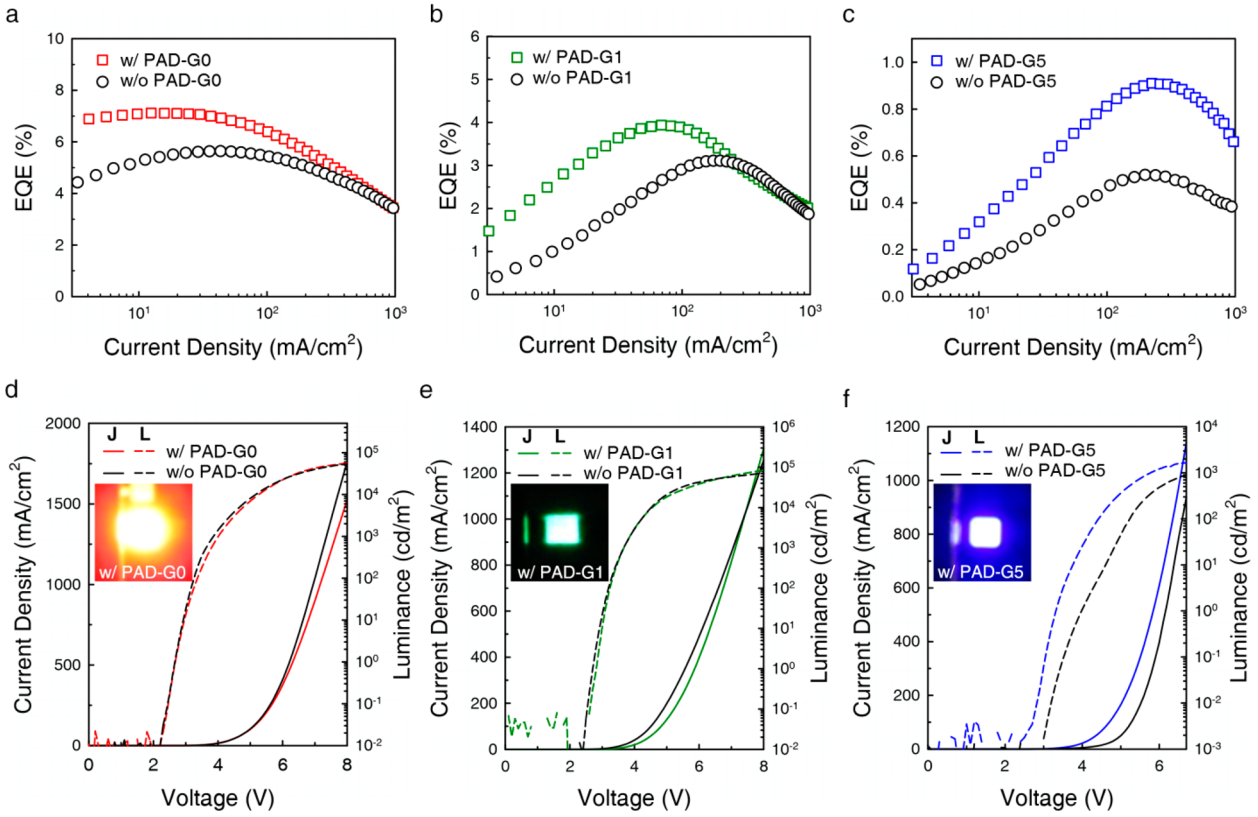

Figure 3. (a–c) EQE *versus* current density graphs and (d–f) current density–voltage–luminance characteristics for QLEDs employing (a, d) CdSe(r = 2 nm)/$Cd_{1-x}Zn_xS$(h = 6 nm) red-emitting QDs, (b, e) $Cd_{1-x}Zn_xSe$(r = 1.5 nm)/ZnS(h = 6.2 nm) green-emitting QDs and (c, f) $Cd_{1-x}Zn_xS$(r = 2 nm)/ZnS(h = 2.3 nm) blue-emitting QDs with native ligands (OA, black) *versus* charge injection controlling ligands (w/ PAD-Gn). The insets of (d–f) are photographs of red, green, and blue-emitting QLEDs (at a current density of 10 mA/cm²) with PAD ligands.

Table 3. Device Characteristics of QLEDs Employing CdSe(r = 2 nm)/$Cd_{1-x}Zn_xS$(h = 6 nm) Red-Emitting QDs, $Cd_{1-x}Zn_xSe$(r = 1.5 nm)/ZnS(h = 6.2 nm) Green-Emitting QDs, and $Cd_{1-x}Zn_xS$(r = 2 nm)/ZnS(h = 2.3 nm) Blue-Emitting QDs with Native Ligands (OA) and with PAD Ligands[a]

QDs	ligands	λ_{max}	V_{ON}	max EQE (%)	max CE (cd/A)	max PE (lm/W)	L (cd/m²) @ 10 mA/cm²
CdSe/$Cd_{1-x}Zn_xS$	OA	628	2.1	5.64	6.99	5.29	540.11
	PAD-G0	628	2.1	7.12	8.93	7.76	863.41
CdCd$_{1-x}$Zn$_x$Se/ZnS	OA	520	2.4	3.11	10.58	7.14	396.11
	PAD-G1	520	2.4	3.94	13.43	9.62	1127.87
$Cd_{1-x}Zn_xS$/ZnS	OA	445	2.9	0.52	0.13	0.07	3.33
	PAD-G5	445	2.7	0.91	0.22	0.14	7.92

[a]Abbreviations: wavelength of maximum EL peak intensities (λ_{max}), turn-on voltage (V_{ON}), current efficiency (CE), power efficiency (PE) and luminance (L).

noted that the energy levels of QDs, meanwhile, remain almost unaffected regardless of the ligand layers (*i.e.*, 0.05 eV, Figure S9). Electron injection from the ZnO ETL into QDs can take place under zero bias, whereas the hole injection from the organic HTL into QDs requires the assistance of an external electric field (Figure 2f).[25] The imbalance between electron and hole injection rates yields the presence of excessive electrons within the QD emissive layers, elevating the possibility of nonradiative AR processes. The negative charging and subsequent AR processes are known to be the efficiency-limiting factor particularly for QLEDs with CdSe/CdS quasi-type II QDs, in which the CdSe core is protected by a CdS shell with a conduction band edge energy offset of approximately 20 meV. The introduction of PAD ligands at the interface of the ZnO ETL and CdSe/CdS QDs induces the development of an energetic barrier for electron injection by up-shifting the conduction band edge energy level and the Fermi level of the surface of the ZnO ETL by at most 0.5 eV. The relocation of the energy levels helps balance the charge injection rates from the CTLs into QDs, suppress the nonradiative AR events in QDs, and thus enhance the luminance efficiency of QDs in devices.

Because PAD ligands improve the charge injection balance by modifying the electronic energy levels of the ZnO ETL, the use of PAD ligands is expected to enhance the device performance of QLEDs with different types of QDs, whose energy levels are rested similar to the case of CdSe/CdS QDs (Figure S11). Figure 3 displays the performance of QLEDs employing type I heterostructured QDs with various emission colors (*i.e.*, CdSe(r = 2 nm)/$Cd_{1-x}Zn_xS$(h = 6 nm),[26]

DOI: 10.1021/acsnano.6b07028
ACS Nano 2017, 11, 684–692

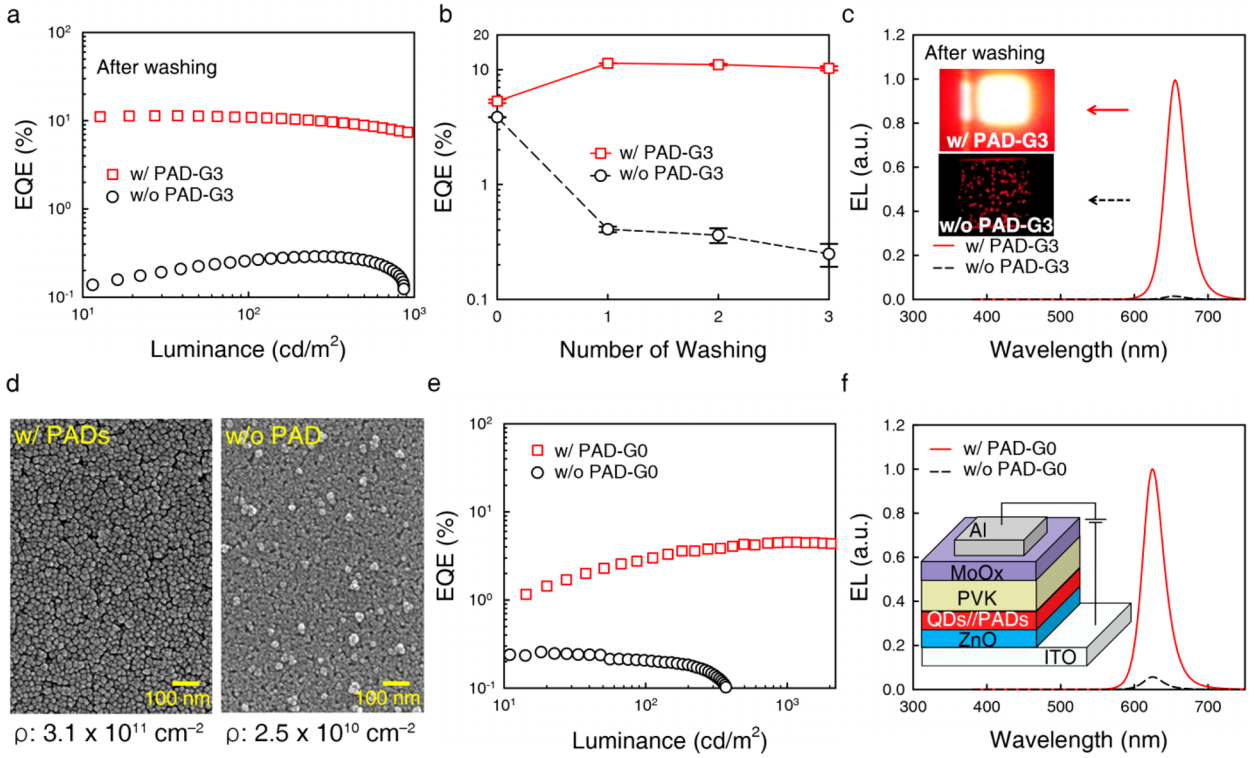

Figure 4. (a) Representative EQE graphs after washing (× 1) QD emissive layers with toluene, (b) peak EQEs as the number of washing processes, and (c) EL spectra (at a current density of 10 mA/cm^2) of QLEDs with native ligands (black) and with charge controlling ligands (PAD-G3, red). (d) Top view SEM images of the QD emissive layers with PAD-G3 (right) and native ligands (left) after washing with toluene. The QD densities (ρ) were counted from SEM images. (e) EQE *versus* luminance and (f) EL spectra (at a current density of 10 mA/cm^2) of QLED with solution-processed HTL. The inset illustrates the device structure of QLED with solution-processed HTL.

$Cd_{1-x}Zn_xSe$(r = 1.5 nm)/ZnS(h = 6.2 nm),[19] and $Cd_{1-x}Zn_xS$(r = 2 nm)/ZnS(h = 2.3 nm)[23] for red, green, and blue-emitting QDs, respectively) (Figure 3, Table 3, Figures S11−12). The peak device efficiencies of QLEDs show 26%, 27%, and 75% improvement for red, green, and blue-emitting QDs, respectively, validating the influence of ligand modification on the improvement of the charge balance within QD emissive layers. We note that the enhancement in the device efficiency for type I heterostructured QDs is apparent, but the outcome is not as dramatic as the case of CdSe/CdS quasi-type II QDs. We attribute this to the presence of thick inorganic shells with larger conduction band energy offsets (*ca.* 0.3 eV) from the emissive cores that prescreen the electron overflow from the ZnO ETL into QDs,[25] similar to the ligand modification layers in the present study. However, thick-inorganic shells inevitably involve suppression of hole injection rates as well and often yield an increase in the operation voltage, which is detrimental to the device performance (Figure S12). Ligand modification *via* the partial ligand exchange method, in contrast, enables the selective adjustment of the injection rate of each type of charge carrier and enhances the charge balance without unwanted drawbacks.

In addition to the charge injection controlling layer, PAD ligands function as a strong linker between QD emissive layers and the underlying ZnO ETL and thereby endow QD emissive layers with structural robustness against consecutive solution processing methods. Figure 4 distinctly contrasts the structural robustness of QD emissive layers with the modified ligands (PAD-G3) *versus* native ligands (OA). The device efficiency of QLEDs based on QDs with native ligands drops substantially after exposure to the solvent (*i.e.*, spin-casting with toluene) because of the removal of QD emissive layers (Figure 4a−d). In contrast, the device efficiency of QLEDs with the ligand modification layer increases after the first washing step and remains unaffected during repeated solvent exposure (Figure 4a−d). The increase in the device efficiency after the first washing step is attributed to the removal of residual OAs after the ligand exchange processing and weakly bound QDs, which otherwise would interrupt efficient charge carrier injection and deteriorate the charge balance. We remark that the result observed from the present study, the best efficiency of QLED from the QD monolayer, agrees with the previous experimental result, corroborating that the compact QD monolayer performs as an effective exciton recombination zone in QLEDs utilizing core/shell heterostructured QDs.[38]

Finally, as a feasibility study for all-solution-processed QLEDs, we fabricated inverted QLEDs employing a solution-processed HTL layer (poly(9-vinylcarbazole), 30 nm) on top of a ZnO ETL//QD emissive layer (Figure 4e, f). QLEDs with charge injection controlling ligands show a peak EQE of 4.5% at a luminance of over 1000 cd/m^2, which surpasses the device performance of QLEDs with QDs of native ligands (peak EQE of below 0.26%). Although the test performance falls below that of QLEDs with thermally evaporated HTLs (EQE = 11.36%), it still outperforms that of the reference QLED with pristine QDs (EQE = 3.86%). We believe that the advance in soluble HTLs and optimization of the device architecture will enable all-solution-processed QLEDs with device performance comparable to or better than that of QLEDs employing thermally evaporated HTLs.

DOI: 10.1021/acsnano.6b07028
ACS Nano 2017, 11, 684−692

CONCLUSION

In summary, we demonstrated multifunctional dendrimer ligand modification that helps achieve controllability of the charge injection rate as well as the structural robustness of QD emissive layers. The spectroscopic analysis in conjunction with the device characterization unveiled the role of the modified multibranched dendrimer ligands in the adjustment of charge injection rate and the device performance. We observed a substantial enhancement in the device performance as well as the feasibility of all-solution-processed QLEDs on a platform of ligand modification. This simple ligand-exchange process resonates profoundly, as the approach highlights both the importance of controlling the ligands of QDs to enhance QLED performance and the feasibility of using the chemical approach toward all-solution-processed QLEDs.

EXPERIMENTAL METHODS

Chemicals. Zinc acetate ($Zn(acet)_2$, 99.99%, metals basis), 1-octadecene (ODE, 90%), and tri-*n*-octylphosphine (TOP, ≥99%) were purchased from UniAm (Korea). Cadmium oxide (CdO, 99.95%, metals basis), Se (99.99%, powder), S (99.998%, powder), oleic acid (OA, 90%), 1-dodecanethiol (DDT, ≥ 98%), and myristic acid (MA, ≥ 99%) were obtained from Alfa Aesar. Poly(amidoamine) dendrimers, ethanolamine (99.5%), and 2-methoxyethanol (99.8%) were acquired from Sigma-Aldrich. All organic solvents were used as received from Daejung (Korea) without purification.

QD Precursors. Cationic precursors (0.5 M cadmium oleate ($Cd(OA)_2$) and 0.5 M zinc oleate ($Zn(OA)_2$)) were prepared by degassing 100 mmol of CdO (or $Zn(acet)_2$) in a mixed solution of 100 mL of OA and 100 mL of ODE at 110 °C for 2 h, followed by backfilling with Ar. The reaction flask was then heated up to 250 °C for 1 h, degassed at 110 °C for 2 h, and backfilled with Ar. Anionic precursors [2 M selenium in tri-*n*-octylphosphine (TOPSe) and 2 M sulfur in tri-*n*-octylphosphine (TOPS)] were prepared by dissolving 20 mmol of selenium and sulfur power in 10 mL of TOP under Ar atmosphere at 100 °C for 1 h. 0.5 M DDT precursor was prepared by diluting 10 mmol of DDT in ODE with a total volume of 20 mL.

Synthesis of QDs. All QD synthesis was conducted with a typical Schlenk line technique under Ar atmosphere. For CdSe(r = 2 nm)/CdS(h = 6 nm) QDs, we first synthesized CdSe core with a radius of 2 nm and separately conducted CdS shelling by supplying desired amounts of 0.5 M $Cd(OA)_2$ and 0.5 M DDT into the reaction vessel containing the CdSe core solution (1 g of CdSe core in 15 mL of ODE) at a rate of 2 mL/h. The reaction temperature was maintained at 300 °C throughout the CdS shelling process. The resultant QDs were purified five times *via* the precipitation/redispersion method and dispersed in toluene for further experiments. Detailed synthetic procedures for CdSe(r = 2 nm)/$Cd_{1-x}Zn_xS$(h = 6 nm) red-emitting QDs, $Cd_{1-x}Zn_xSe$(r = 1.5 nm)/ZnS(h = 6.2 nm) green-emitting QDs, and $Cd_{1-x}Zn_xS$(r = 2 nm)/ZnS(h = 2.3 nm) blue-emitting QDs and their structural and optical properties are provided in Supporting Information.

Device Fabrication. ZnO films were prepared using a previously reported method[29] with minor modifications. Prior to film formation, ZnO precursor was prepared by dissolving 1 g of $Zn(acet)_2$ and 0.28 g of ethanolamine in 10 mL of 2-methoxyethanol for 12 h. The resulting ZnO precursor was spun-cast on patterned ITO substrates with a spin rate of 3000 rpm for 30 s to form ZnO films. The ZnO films were then annealed at 300 °C under air for 1 h. PAD ligand layers were formed on the ZnO film by spin-casting PAD ligand solutions diluted in ethanol (2 mg/mL) with a spin-rate of 4000 rpm for 30 s. The weakly bound PAD ligands were washed by spin-casting PAD//ZnO substrates with pure ethanol under the same spin condition. QD dispersions (20 mg/mL in toluene) were then deposited on PAD//ZnO substrates at 4000 rpm for 30 s, followed by a washing step (spin-casting with pure toluene at 4000 rpm for 30 s). CBP, MoO_x, and Al electrode layers were thermally evaporated under a vapor pressure of 2 × 10^{-6} Torr onto QD//PAD//ZnO//ITO substrates at deposition rates of 0.8–1 Å·s^{-1}, 0.3 Å·s^{-1}, and 4–5 Å·s^{-1}, respectively. For solution-processed QLEDs, poly(9-vinylcarbazole) (PVK) dissolved in chlorobenzene at a concentration of 15 mg/mL was spun-cast onto QD//PAD//ZnO//ITO substrates at 3000 rpm for 60 s and annealed at 140 °C for 30 min under Ar atmosphere, followed by thermal evaporation of MoO_x and Al electrodes.

Optical Characterization. UV–vis absorption and photoluminescence spectra were obtained with a Lambda 35 spectrometer (PerkinElmer) and Fluoromax-4 spectrometer (Horiba Science), respectively. The absolute PL QYs of film samples were obtained at an excitation wavelength of 450 nm with a C11347–01 (Hamamatsu Photonics). To characterize the PL decay dynamics, the samples were excited at 450 nm (pulse width =80 ps) at a repetition rate of 1.0 MHz, and PL dynamics were resolved using a time-correlated single-photon counting (TCSPC) system that consists of a single channel analyzer (with a Picoquant Timeharp 260) and avalanche photodiodes (Picoquant τ-SPAD, timing resolution = 350 ps).

Film Characterization. The X-ray photoelectron spectroscopy (XPS) measurements were performed with a ULVAC-PHI X-tool Spectrometer (base pressure of 6.7 × 10^{-7} Pa) equipped with monochromatic Al–Kα X-ray photons ($h\nu$ = 1486.6 eV). Ultraviolet photoelectron spectroscopy (UPS) measurements were conducted with an AXIS-NOVA and Ultra DLD using a He I (21.2 eV for UPS) discharge lamp.

Device Characterization of QLEDs. The current–voltage–luminance (I–V–L) characteristics of the devices were measured with a Keithley-236 source-measure unit, a Keithley-2000 multimeter unit coupled with a calibrated Si photodiode (Hamamatsu S5227–1010BQ) and a photomultiplier tube detector. The luminance and efficiencies of QLEDs were calculated from the photocurrent measurement data obtained with the Si photodiode. The electroluminescence spectra were obtained using a spectroradiometer (CS-2000).

ASSOCIATED CONTENT

Supporting Information

The Supporting Information is available free of charge on the ACS Publications website at DOI: 10.1021/acsnano.6b07028.

Additional experimental details and data (PDF)

AUTHOR INFORMATION

Corresponding Authors

*E-mail: jinhan71@korea.ac.kr.
*E-mail: wkbae@kist.re.kr.

ORCID

Byeong Guk Jeong: 0000-0002-0544-364X
Doh C. Lee: 0000-0002-3489-6189
Wan Ki Bae: 0000-0002-3832-2449

Author Contributions

‖These authors contributed equally to this work.

Notes

The authors declare no competing financial interest.

ACKNOWLEDGMENTS

This work was supported by Samsung Research Funding Center of Samsung Electronics under Project Number SRFC-MA1301-07. W.K.B. acknowledges the Ministry of Trade, Industry & Energy (MOTIE, 10051541) and Korea Display Research Consortium (KDRC) support program for the development of future devices technology for display industry. D.C.L. acknowledges the National Research Foundation (NRF) grants funded by the Korean government (NRF-2016M3A7B4910618). C.H.L. acknowledges Mid-career Re-

DOI: 10.1021/acsnano.6b07028
ACS Nano 2017, 11, 684–692

searcher Program (2016R1A2B3009301) funded by the National Research Foundation of Korea (NRF) and the Industrial Strategic Technology Development Program (10045145) funded by the Ministry of Trade, Industry and Energy (MOTIE).

REFERENCES

(1) Klimov, V. I. *Nanocrystal Quantum Dots*; CRC Press; Taylor and Francis Group: Boca Raton, FL, 2010.
(2) Brus, L. Electronic Wave Functions in Semiconductor Clusters: Experiment and Theory. *J. Phys. Chem.* **1986**, *90*, 2555−2560.
(3) Alivisatos, A. P. Perspectives on the Physical Chemistry of Semiconductor Nanocrystals. *J. Phys. Chem.* **1996**, *100*, 13226−13239.
(4) Murray, C. B.; Kagan, C. R.; Bawendi, M. G. Synthesis and Characterization of Monodisperse Nanocrystals and Close-Packed Nanocrystal Assemblies. *Annu. Rev. Mater. Sci.* **2000**, *30*, 545−610.
(5) Colvin, V. L.; Schlamp, M. C.; Alivisatos, A. P. Light-Emitting Diodes Made from Cadmium Selenide Nanocrystals and a Semiconducting Polymer. *Nature* **1994**, *370*, 354−357.
(6) Klimov, V. I.; Mikhailovsky, A. A.; Xu, S.; Malko, A.; Hollingsworth, J. A.; Leatherdale, C. A.; Eisler, H.-J.; Bawendi, M. G. Optical Gain and Stimulated Emission in Nanocrystal Quantum Dots. *Science* **2000**, *290*, 314−317.
(7) Chan, W. C. W.; Nie, S. Quantum Dot Bioconjugates for Ultrasensitive Nonisotopic Detection. *Science* **1998**, *281*, 2016−2018.
(8) Meinardi, F.; Colombo, A.; Velizhanin, K. A.; Simonutti, R.; Lorenzon, M.; Beverina, L.; Viswanatha, R.; Klimov, V. I.; Brovelli, S. Large-Area Luminescent Solar Concentrators Based on 'Stokes-Shift-Engineered' Nanocrystals in a Mass-Polymerized PMMA Matrix. *Nat. Photonics* **2014**, *8*, 392−399.
(9) Coe, S.; Woo, W.-K.; Bawendi, M.; Bulovic, V. Electroluminescence from Single Monolayers of Nanocrystals in Molecular Organic Devices. *Nature* **2002**, *420*, 800−803.
(10) Achermann, M.; Petruska, M. A.; Koleske, D. D.; Crawford, M. H.; Klimov, V. I. Nanocrystal-Based Light-Emitting Diodes Utilizing High-Efficiency Nonradiative Energy Transfer for Color Conversion. *Nano Lett.* **2006**, *6*, 1396−1400.
(11) Kwak, J.; Bae, W. K.; Lee, D.; Park, I.; Lim, J.; Park, M.; Cho, H.; Woo, H.; Yoon, D. Y.; Char, K.; Lee, S.; Lee, C. Bright and Efficient Full-Color Colloidal Quantum Dot Light-Emitting Diodes Using an Inverted Device Structure. *Nano Lett.* **2012**, *12*, 2362−2366.
(12) Castelli, A.; Meinardi, F.; Pasini, M.; Galeotti, F.; Pinchetti, V.; Lorenzon, M.; Manna, L.; Moreels, I.; Giovanella, U.; Brovelli, S. High-Efficiency All-Solution-Processed Light-Emitting Diodes Based on Anisotropic Colloidal Heterostructures with Polar Polymer Injecting Layers. *Nano Lett.* **2015**, *15*, 5455−5464.
(13) Lim, J.; Park, M.; Bae, W. K.; Lee, D.; Lee, S.; Lee, C.; Char, K. Highly Efficient Cadmium-Free Quantum Dot Light-Emitting Diodes Enabled by the Direct Formation of Excitons within InP@ZnSeS Quantum Dots. *ACS Nano* **2013**, *7*, 9019−9026.
(14) Dai, X.; Zhang, Z.; Jin, Y.; Niu, Y.; Cao, H.; Liang, X.; Chen, L.; Wang, J.; Peng, X. Solution-Processed, High-Performance Light-Emitting Diodes Based on Quantum Dots. *Nature* **2014**, *515*, 96−99.
(15) Talapin, D. V.; Lee, J. S.; Kovalenko, M. V.; Shevchenko, E. V. Prospects of Colloidal Nanocrystals for Electronic and Optoelectronic Applications. *Chem. Rev.* **2010**, *110*, 389−458.
(16) Bae, W. K.; Kwak, J.; Park, J. W.; Char, K.; Lee, C.; Lee, S. Highly Efficient Green-Light-Emitting Diodes Based on CdSe@ZnS Quantum Dots with a Chemical-Composition Gradient. *Adv. Mater.* **2009**, *21*, 1690−1694.
(17) Shen, H.; Cao, W.; Shewmon, N. T.; Yang, C.; Li, L. S.; Xue, J. High-Efficiency, Low Turn-on Voltage Blue-Violet Quantum-Dot-Based Light-Emitting Diodes. *Nano Lett.* **2015**, *15*, 1211−1216.
(18) Yang, Z.; Voznyy, O.; Liu, M.; Yuan, M.; Ip, A. H.; Ahmed, O. S.; Levina, L.; Kinge, S.; Hoogland, S.; Sargent, E. H. All-Quantum-Dot Infrared Light-Emitting Diodes. *ACS Nano* **2015**, *9*, 12327−12333.
(19) Bae, W. K.; Char, K.; Hur, H.; Lee, S. Single-Step Synthesis of Quantum Dots with Chemical Composition Gradients. *Chem. Mater.* **2008**, *20*, 531−539.
(20) Li, J. J.; Wang, A.; Guo, W.; Keay, J. C.; Mishima, T. D.; Johnson, M. B.; Peng, X. Large-Scale Synthesis of Nearly Monodisperse CdSe/CdS Core/Shell Nanocrystals Using Air-Stable Reagents *via* Successive Ion Layer Adsorption and Reaction. *J. Am. Chem. Soc.* **2003**, *125*, 12567−12575.
(21) Lim, J.; Bae, W. K.; Lee, D.; Nam, M. K.; Jung, J.; Lee, C.; Char, K.; Lee, S. InP@ZnSeS, Core@Composition Gradient Shell Quantum Dots with Enhanced Stability. *Chem. Mater.* **2011**, *23*, 4459−4463.
(22) Akselrod, G. M.; Prins, F.; Poulikakos, L. V.; Lee, E. M. Y.; Weidman, M. C.; Mork, A. J.; Willard, A. P.; Bulovic, V.; Tisdale, W. A. Subdiffusive Exciton Transport in Quantum Dot Solids. *Nano Lett.* **2014**, *14*, 3556−3562.
(23) Bae, W. K.; Nam, M. K.; Char, K.; Lee, S. Gram-Scale One-Pot Synthesis of Highly Luminescent Blue Emitting $Cd_{1-x}Zn_xS$/ZnS Nanocrystals. *Chem. Mater.* **2008**, *20*, 5307−5313.
(24) Bae, W. K.; Padilha, L. A.; Park, Y.-S.; McDaniel, H.; Robel, I.; Pietryga, J. M.; Klimov, V. I. Controlled Alloying of the Core-Shell Interface in CdSe/CdS Quantum Dots for Suppression of Auger Recombination. *ACS Nano* **2013**, *7*, 3411−3419.
(25) Bae, W. K.; Park, Y.-S.; Lim, J.; Lee, D.; Padilha, L. A.; McDaniel, H.; Robel, I.; Lee, C.; Pietryga, J. M.; Klimov, V. I. Controlling the influence of Auger recombination on the performance of quantum-dot light-emitting diodes. *Nat. Commun.* **2013**, *4*, 2661.
(26) Lim, J.; Jeong, B. G.; Park, M.; Kim, J. K.; Pietryga, J. M.; Park, Y.-S.; Klimov, V. I.; Lee, C.; Lee, D. C.; Bae, W. K. Influence of Shell Thickness on the Performance of Light-Emitting Devices Based on CdSe/$Zn_{1-x}Cd_xS$ Core/Shell Heterostructured Quantum Dots. *Adv. Mater.* **2014**, *26*, 8034−8040.
(27) Ko, Y.; Baek, H.; Kim, Y.; Yoon, M.; Cho, J. Hydrophobic Nanoparticle-Based Nanocomposite Films Using In Situ Ligand Exchange Layer-by-Layer Assembly and Their Nonvolatile Memory Applications. *ACS Nano* **2013**, *7*, 143−153.
(28) Kim, D.; Cheong, S.; Ahn, Y. G.; Ryu, S. W.; Kim, J.-K.; Cho, J. Multicatalytic Colloids with Highly Scalable, Adjustable, and Stable Functionalities in Organic and Aqueous Media. *Nanoscale* **2016**, *8*, 7000−7016.
(29) Sun, Y.; Seo, J. H.; Takacs, C. J.; Seiter, J.; Heeger, A. J. Inverted Polymer Solar Cells Integrated with a Low Temperature-Annealed Sol-Gel-Derived ZnO Film as an Electron Transport Layer. *Adv. Mater.* **2011**, *23*, 1679−1683.
(30) Wang, Q.; Ma, D. Management of Charges and Excitons for High-Performance White Organic Light-Emitting Diodes. *Chem. Soc. Rev.* **2010**, *39*, 2387−2398.
(31) Bozyigit, D.; Yarema, O.; Wood, V. Origins of Low Quantum Efficiencies in Quantum dot LEDs. *Adv. Funct. Mater.* **2013**, *23*, 3024−3029.
(32) Bae, W. K.; Brovelli, S.; Klimov, V. I. Spectroscopic Insights into the Performance of Quantum Dot Light-Emitting Diodes. *MRS Bull.* **2013**, *38*, 721−730.
(33) Pietryga, J. M.; Park, Y.-S.; Lim, J.; Fidler, A. F.; Bae, W. K.; Brovelli, S.; Klimov, V. I. Spectroscopic and Device Aspects of Nanocrystal Quantum Dots. *Chem. Rev.* **2016**, *116*, 10513−10622.
(34) Brovelli, S.; Schaller, R. D.; Crooker, S. A.; Garcia-Santamaria, F.; Chen, Y.; Viswanatha, R.; Hollingsworth, J. A.; Htoon, H.; Klimov, V. I. Nano-Engineered Electron-Hole Exchange Interaction Controls Exciton Dynamics in Core-Shell Semiconductor Nanocrystals. *Nat. Commun.* **2011**, *2*, 280.
(35) Pal, B. N.; Ghosh, Y.; Brovelli, S.; Laocharoensuk, R.; Klimov, V. I.; Hollingsworth, J. A.; Htoon, H. 'Giant' CdSe/CdS Core/Shell Nanocrystal Quantum Dots As Efficient Electroluminescent Materials: Strong Influence of Shell Thickness on Light-Emitting Diode Performance. *Nano Lett.* **2012**, *12*, 331−336.
(36) Zhou, Y.; Fuentes-Hernandez, C.; Shim, J.; Meyer, J.; Giordano, A. J.; Li, H.; Winget, P.; Papadopoulos, T.; Cheun, H.; Kim, J.; Fenoll, M.; Dindar, A.; Haske, W.; Najafabadi, E.; Khan, T. M.; Sojoudi, H.; Barlow, S.; Graham, S.; Bredas, J.-L.; Marder, S. R.; et al. A Universal

DOI: 10.1021/acsnano.6b07028
ACS Nano 2017, 11, 684−692

Method to Produce Low-Work Function Electrodes for Organic Electronics. *Science* **2012**, *336*, 327−332.
(37) Woo, S.; Kim, W. H.; Kim, H.; Yi, Y.; Lyu, H.-K.; Kim, Y. 8.9% Single-Stack Inverted Polymer Solar Cells with Electron-Rich Polymer Nanolayer-Modified Inorganic Electron-Collecting Buffer Layers. *Adv. Energy Mater.* **2014**, *4*, 1301692.
(38) Bae, W. K.; Kwak, J.; Lim, J.; Lee, D.; Nam, M. K.; Char, K.; Lee, C.; Lee, S. Multicolored Light-Emitting Diodes Based on All-Quantum-Dot Multilayer Films Using Layer-by-Layer Assembly Method. *Nano Lett.* **2010**, *10*, 2368−2373.

DOI: 10.1021/acsnano.6b07028
ACS Nano 2017, 11, 684−692